


The Influence of Rheological and Wetting Properties of Hydrogel-based Bio-Inks on Extrusion-based Bioprinting

Bruna Regina Maciel*, Kubilay Baki, Claude Oelschlaeger, and Norbert Willenbacher

DOI: 10.1002/cite.202100139

 This is an open access article under the terms of the Creative Commons Attribution-NonCommercial-NoDerivs License, which permits use and distribution in any medium, provided the original work is properly cited, the use is non-commercial and no modifications or adaptations are made.

Dedicated to Prof. Dr. Thomas Hirth on the occasion of his 60th birthday

The wall slip and flow behavior of alginate as well as gelatin based hydrogels with respect to the impact of these rheological and wetting properties on extrusion-based bioprinting (EBB) was investigated. Capillary rheometry and printing tests indicate that slip is negligible at high stresses relevant for EBB, i.e., well above the hydrogels yield stress. On the contrary, rotational rheometry performed at low shear stresses revealed that alginate hydrogels present much stronger slip than gelatin gels, irrespective of crosslinker and polymer concentration. This result is presumably due to the formation of a heterogeneous microstructure for alginate gels and has an unfavorable impact on the printing quality with the production of large fluctuations in line width and higher line spread ratio.

Keywords: Alginate, Gelatin, Rheology, 3D bioprinting, Wall slip

Received: July 22, 2021; *revised:* October 08, 2021; *accepted:* November 29, 2021

1 Introduction

Bioprinting enables the deposition of living cells at specific positions in the printed scaffold, forming three dimensional constructs that mimic the human tissue micro-environment [1, 2]. This 3D configuration enhances cell proliferation similarly to the one of the living tissue, which may not be the case for most 2D cell culture methods [3, 4]. The most commonly employed techniques for bioprinting are the extrusion-based bioprinting (EBB), material jetting or inkjet bioprinting as well as vat polymerization (VP) [1]. Although material jetting and vat polymerization bioprinting both offer higher printing resolution ($< 100\mu\text{m}$) in comparison to EBB, low viscosity materials are required for inkjet bioprinting (3–30 mPa s) and nozzle clogging is a recurrent issue [5, 6]. Moreover, VP bioprinting struggles with the limited choice of photo-curable biomaterials and use of single bio-resin [5]. EBB, on the other hand, is widely used due to its versatility, affordability and facility to operate [7]. EBB allows a broad range of bioinks viscosity (30– 10^7 mPa s) to be printed, as well as a higher throughput rate in comparison to the other techniques [1]. During the pneumatic EBB process, a mixture of living cells and a carrier material is extruded through a nozzle controlled by an external pressure. This mixture is the so called bioink. Biocompatible polymeric hydrogels are often used as cell carrier materials [8, 9]. Due to their high water content, hydrogels are prone to wall slip under flow [10, 11]. Slip behavior occurs when a thin liquid layer is

formed between the wall and the hydrogel, apparently invalidating the often tacitly assumed no-slip assumption. Slip flow can be controlled by employing wall materials with different wettability properties [12–14]. Precision nozzles made from stainless steel are widely used for bioprinting [15, 16]. Nevertheless, nozzles made of polymers, such as polytetrafluoroethylene (PTFE) and polypropylene (PP) are also found on the market. The flow behavior through the nozzle during bioprinting was studied for shear thinning materials considering that the no-slip condition is valid [15, 17–19]. The effect of wall slip on nozzle flow and printing behavior of biopolymer solutions has also been investigated [20, 21]. These studies, however, rely on a narrow range of shear rate controlled rheological measurements not taking into account that the slip velocity generally strongly depends on the applied stress [22].

Herein the phenomenon of wall slip on EBB quality using two different types of bioinks, namely alginate- and gelatin-based hydrogels, is discussed. First, rotational rheometry experiments employing parallel-plate geometries made of different materials, i.e., with different surface energy values,

Bruna Regina Maciel, Kubilay Baki, Dr. Claude Oelschlaeger,
Prof. Dr. Norbert Willenbacher
bruna.maciel@kit.edu

Karlsruhe Institute of Technology (KIT), Institute for Mechanical
Process Engineering and Mechanics, Gotthard-Franz-Strasse 3,
Building 50.31, 76131 Karlsruhe, Germany.

namely PTFE, polypropylene, and stainless steel, were performed. In this case, the wall slip velocity under controlled shear stress conditions similar as in an EBB experiment was determined. The accessible absolute stress values, however, are lower than typically applied during printing. Additionally, rotational rheometry was used to determine the yield stress and the elastic shear modulus of the hydrogels. Then, capillary rheometry was used to study the flow behavior under high shear conditions similar to those of EBB. In this case only stainless steel capillaries were used. Finally, 3D printing experiments with nozzles made of different materials were performed. The line resolution, shape fidelity, and stability of multi-layered constructs post-printing were systematically determined. The results help to understand how wall slip, yield stress, and elastic shear modulus of bioinks are related to the printing quality and will promote the development of tailor-made bioprinting strategies.

2 Materials and Methods

2.1 Sample Preparation

Sodium alginate (alginic acid sodium salt from brown algae, BioReagent) and poly(vinyl alcohol) (PVA, Mowiol[®] 4-98) were purchased from Sigma- Aldrich Chemie GmbH (Taufkirchen, Germany). Gelatin extra pure, gold, 180 Bloom, calcium chloride (CaCl_2) > 98 % dehydrated and calcium sulfate (CaSO_4) > 98 % dihydrate were purchased from Carl Roth (Karlsruhe, Germany). D-Glucono-1,5-lacton (GDL) > 99 % was purchased from Alfa Aesar (Thermo Fischer, Karlsruhe, Germany). Calcium carbonate (CaCO_3 , Ulmer Weiss 15H) was purchased from Eduard Merkle GmbH (Blaubeuren-Altental, Germany). Alginate, CaCl_2 , CaSO_4 , and GDL solutions were prepared stirring the powder with Milli-Q water at room temperature until they appeared limpid and homogeneous. Gelatin and PVA solutions were prepared using the same procedure, but stirring occurred at 40 and 90 °C, respectively. CaCO_3 suspension was prepared stirring the powder with Milli-Q water. Alginate samples A and B were prepared by mixing alginate solution with the salt solution. GDL was added to sample B in order to dissolve CaCO_3 . Sample C was composed of only gelatin solution and sample D of gelatin mixed with PVA solution. Tab. 1 shows the composition details and final weight concentrations of the different ingredients for the investigated bioink systems:

Table 1. Composition of alginate and gelatin-based samples.

| | Alginate-based | | Gelatin-based | |
|-------------|------------------------|--|---------------|-----------------------|
| | A | B | C | D |
| Polymer | 1.3 % Alginate | 1.3 % Alginate | 4 % Gelatin | 8 % Gelatin + 2 % PVA |
| Crosslinker | 0.17 % CaSO_4 | 0.13 % CaCl_2 + 0.04 % CaCO_3 + 0.04 % GDL | - | - |

2.2 Rotational Rheometry

A rotational rheometer (Rheoscope I, Thermo Haake, Karlsruhe, Germany), equipped with a stainless steel plate-plate measuring cell (diameter 20 mm, roughness $R_z = 2.1 \pm 0.3 \mu\text{m}$) was used to perform steady as well as small amplitude oscillatory shear experiments at 20 °C. The storage modulus G' of gels is typically independent of the applied frequency of shear deformation. Here this plateau value of G' , also called shear modulus G_0 , was determined as the value of the storage modulus G' at an angular frequency of 1 rad s^{-1} . Plates of different materials, namely polytetrafluoroethylene (PTFE, $R_z = 3.2 \pm 0.3 \mu\text{m}$), polypropylene (PP, $R_z = 1.9 \pm 0.5 \mu\text{m}$) and sandpaper P320 ($R_z = 59 \pm 16 \mu\text{m}$) were also attached to the plate-plate fixture. Laser scanning microscopy (VK-X100 Keyence, Neu-Isenburg, Germany) was used to assess the roughness of the disk plates. Crosslinked hydrogels are solid-like materials at rest and a critical stress, generally termed apparent yield stress, has to be exceeded to enable flow [23]. Pronounced slip behavior often limits rheological characterization of hydrogels. Accordingly, plate fixtures with increased roughness are often used in rotational rheometry [24, 25]. Here, yield stress determination was done based on creep tests employing the attached sandpaper disk. The shear stress was stepwise increased from 1 to 1000 Pa. The yield stress was determined using the two-tangent method where deformation was plotted as a function of shear stress using logarithmic scales. Then, one tangent is fitted to the data in the low shear, elastic response regime while the second tangent is fitted to the plastic deformation region. The value extracted from the crossover of the two tangents is the yield stress [26]. Similar stress ramps were also applied to assess the slip behavior with the smooth plate-plate fixtures. Video recordings were performed using an objective borescope and a Digital Microscope VHX-950F Keyence (Neu-Isenburg, Germany) in order to visualize the deformation of the sample rim.

2.3 Capillary Rheometry

High shear viscosity data were determined at 20 °C using a self-assembled piston-driven capillary rheometer. The samples were forced to flow through stainless steel capillaries with different diameter (0.5–1.5 mm) and lengths (30–90 mm) at controlled volumetric flow rates corresponding to constant shear rate values using a piston of 20 mm diameter. The resulting extrusion pressure was recorded using a pressure transducer (0–50 bar, Dynisco Europe GmbH, Heilbronn, Germany).

2.4 3D Printing of Hydrogels

The alginate and gelatin-based hydrogels were stained with blue ink (Pelikan, Berlin, Germany) for better visibility and printed on microscope glass slides using a pressure-controlled Voxel 8 Developer's Kit 3D printer (Voxel 8 Inc., Harvard, USA). 3CC cartridges (Nordson EFD, Feldkirchen, Germany) and straight needles of different materials, namely stainless steel, PTFE and PP (250 μm outlet diameter and 18 mm length, VIEWEG, Germany), were used to extrude the hydrogels in a log pile pattern. The print head velocity was kept at 600 mm min^{-1} for all samples. The 3D constructs were imaged using a Digital Microscope VHX-950F (Keyence, Neu-Isenburg, Germany) and image analysis was performed with the software Image Processing System (Visiometrics iPS).

3 Results and Discussion

3.1 Rotational Rheometry: Low Shear Stress

3.1.1 Slip Stress Visualization and Slip Velocity Determination

The slip behavior of alginate and gelatin-based hydrogels can be visually observed in the video snapshots in Fig. 1. For sample B, an alginate-based hydrogel (Fig. 1a), no movement of the PTFE upper plate was observed for shear stress values lower than 15 Pa. Above this value, the upper plate starts moving and only a thin layer close to the plate is sheared whereas the rest of the sample remains intact (Fig. 1b). Similar pronounced wall slip behavior was observed for alginate samples A and B in contact with steel and PP plates. For gelatin-based gels C and D only slight slip was detected, e.g., for sample C (Fig. 1c), the stainless steel plate only starts moving at shear stress values above 167 Pa and deformation takes place in the upper half layer

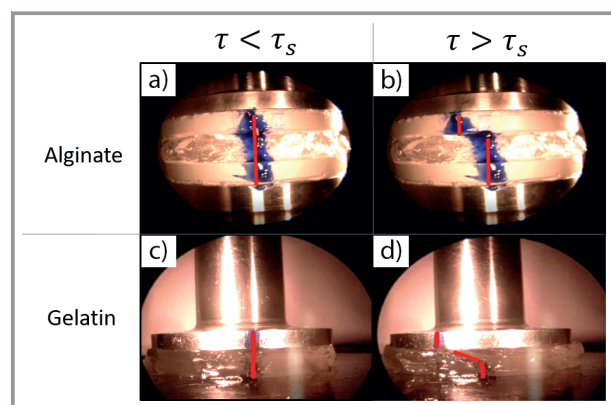


Figure 1. Video snapshots of alginate-based sample B, at $\tau < \tau_s$ (a) and $\tau > \tau_s$ (b) and gelatin-based sample C, at $\tau < \tau_s$ (c) and $\tau > \tau_s$ (d) during shear stress ramp measurement with plate-plate rheometer.

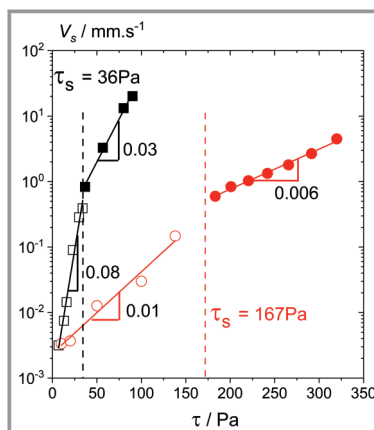


Figure 2. Slip velocity V_s as a function of shear stress τ for alginate-based sample B (squares) and gelatin-based sample C (circles) determined with stainless steel plate-plate fixture. Open symbols refer to data obtained using a modified Yoshimura *et al.* approach based on a variation of gap height (Eq. (1)). Closed symbols refer to data directly calculated from the rotation of the upper plate (Eq. (2)).

of the gel with only little slip (Fig. 1d). Similar minor slip behavior was observed when PTFE and PP plates were used. The shear stress at which the onset of slip can be visually observed is the so-called critical slip stress τ_s [12].

Note that this critical stress τ_s for both types of material is well below the yield stress of the gels obtained with particularly rough plates. This will be discussed below in Sect. 3.3. Moreover, slip even occurs below τ_s although it is not visually observable. Therefore, the approach developed by Yoshimura *et al.* to determine the slip velocity under flow by varying the gap height in a plate-plate rheometer was adapted [22, 27]. In the experiments performed here, the samples deform elastically instead of exhibiting a steady shear flow. Accordingly, instead of obtaining the slip velocity from the slope of shear rate $\dot{\gamma}$ as a function of reciprocal gap height, the following relation is used:

$$\gamma_{\text{app}} = \frac{2V_s t_c}{h} + \gamma \quad (1)$$

Where γ_{app} is the apparent elastic deformation of the hydrogel including slip and γ is the true elastic deformation, t_c is a characteristic time constant, h is the gap height and V_s the slip velocity. The characteristic time constant t_c was considered 1 s for all samples at all shear stresses applied. Slip velocity data obtained for samples B and C are summarized in Fig. 2. Starting at the same low value $V_s \approx 3 \times 10^{-3} \text{ mm s}^{-1}$ slip strongly increases with increasing shear stress for both samples. The slope of this increase in the semi-log plot of V_s vs. τ , however, is much more pronounced for the alginate than for the gelatin sample, whereas the critical stress τ_s at which slip starts to be visually accessible is much higher in the latter case.

For shear stresses higher than the slip stress τ_s , the slip velocity at the rim of the rotating plate is given by:

$$V_s = 2n\pi r \quad (2)$$

where n is the plate rotational velocity and r is the plate radius [12]. This approach is justified by the video recordings discussed above. The onset corresponding data are also shown in Fig. 2. Visual observability of slip corresponds to a slip velocity value $V_s \approx 0.5 \text{ mm s}^{-1}$. For alginate this happens at a much lower stress value than for the gelatin sample, as already pointed out above. Moreover, the increase of V_s with τ is much more pronounced for alginate than for the gelatin gel. For both materials a pronounced kink in the V_s vs. τ curves shows up around τ_s and for both materials the upper limit at which V_s can be determined using a plate-plate rotational rheometer is set by sample spillage which occurs at significantly lower stresses for the alginate than for the gelatin sample.

3.1.2 Effect of Plate-Plate Materials on Slip Stress τ_s

Slip stress τ_s values for samples A–D loaded on different plate-plate geometry materials can be seen in Fig. 3. Overall, samples on stainless steel plates present higher slip stress than on PTFE and PP, except for gelatin sample C. Here the slip stress for steel is almost the same as the one for PP. PTFE plates present in general the lowest slip stress value, except for gelatin sample D where the values for PP and PTFE plates are very similar. This result indicates larger wall slip effects occurring using PTFE plates compared to steel plates. The higher adhesion or friction of the hydrogels to stainless steel can be explained by its higher surface energy ($\sim 43 \text{ mJ m}^{-2}$, [28]) compared to PP and PTFE, which present a surface energy of ~ 33 and $\sim 31.5 \text{ mJ m}^{-2}$ [29], respectively.

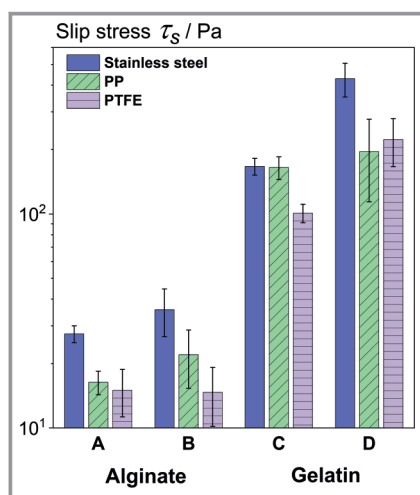


Figure 3. Slip stress τ_s for samples A–D measured with stainless steel plate (blank bars), PP (diagonally patterned bars) and PTFE (horizontally patterned bars).

Another observation is that independent of crosslinker type and sample composition, alginate-based hydrogels are

more susceptible to slip compared to gelatin-based gels. For the alginate samples, slip stress τ_s values are below 40 Pa, whereas for gelatin-based hydrogels τ_s is always larger than 100 Pa. A possible explanation for the difference in wall slip performance might be the distinct chemical composition of alginate (polysaccharide) and gelatin (protein) hydrogels. In an earlier study on food hydrogels, whey protein isolate gels were found to have a higher surface friction than gels containing polysaccharides [30], therefore leading to less slip.

3.1.3 Effect of Sample Composition and Plate-Plate Materials on Slip Velocity V_s

The slip velocity V_s for $\tau > \tau_s$ strongly increases with τ for all samples, as shown in Fig. 4. Both alginate samples A and B share similar dependence of V_s on τ , despite the fact that sample A was crosslinked with CaSO_4 and sample B with a mixture of CaCO_3 and CaCl_2 . The same is observed for gelatin samples C and D, even though sample D has a higher polymer concentration than sample C. No clear trend in the V_s among steel, PP and PTFE plates is observed for samples A–D. Similar results (not shown) were obtained for $\tau < \tau_s$. Overall, slip velocities found for alginate gels are much higher than those found for gelatin samples.

3.2 Capillary Rheometry: High Shear Stress

Capillary rheometry allows us to investigate flow behavior at higher shear rate values, in a range relevant for the 3D printing process (10^3 – 10^5 s^{-1}). Three capillary nozzles of different diameter d and length L , but same ratio $L/d = 30$, were used to extrude the alginate hydrogel at shear rates $> 4 \times 10^2 \text{ s}^{-1}$, with corresponding shear stresses $\tau > 2 \times 10^2 \text{ Pa}$. As can be seen from Fig. 5, the flow behavior of sample B is nozzle size independent, suggesting that slip is negligible at such high shear stress values. Similar results were found for the other samples. In other words, despite the pronounced slip observed at low stress, one can safely neglect wall slip effects at shear stresses relevant during EBB for the alginate and gelatin gels investigated here.

Fig. 6 displays the viscosity of alginate sample B and of gelatin sample C as a function of shear rate. Notably, the samples show pronounced shear thinning and essentially equal viscosity values η in the broad shear rate range covered by combining rotational and capillary rheometry.

3.3 Yield Stress τ_y Determination and Comparison with Slip Stress τ_s

Fig. 7 shows the yield stress τ_y values measured with rough plates for samples A–D in comparison to the critical slip stress τ_s measured with smooth stainless steel plates. In all cases, $\tau_y > \tau_s$. Alginate gels, however, present a larger ratio

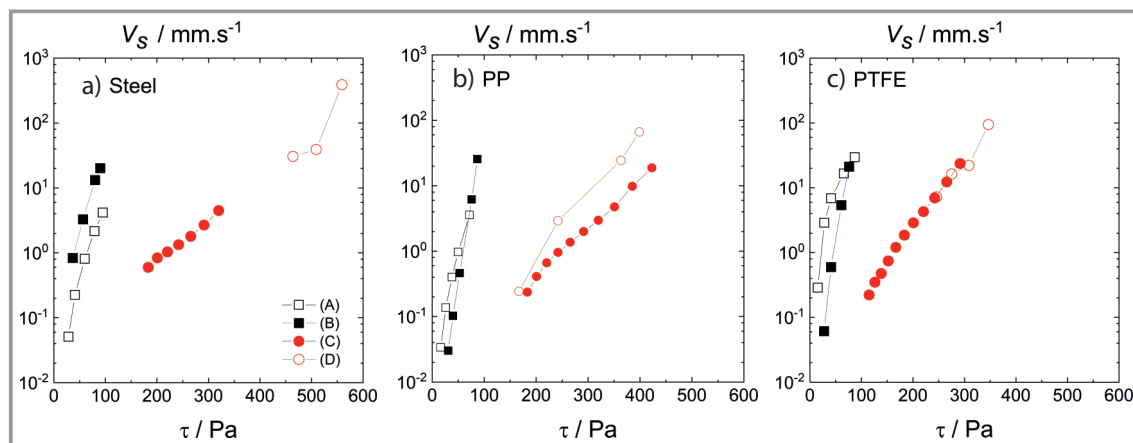


Figure 4. Slip velocity V_s of alginate-based samples A and B and gelatin-based samples C and D as a function of τ for $\tau > \tau_s$, measured using steel (a), PP (b), and PTFE (c) plate-plate geometries.

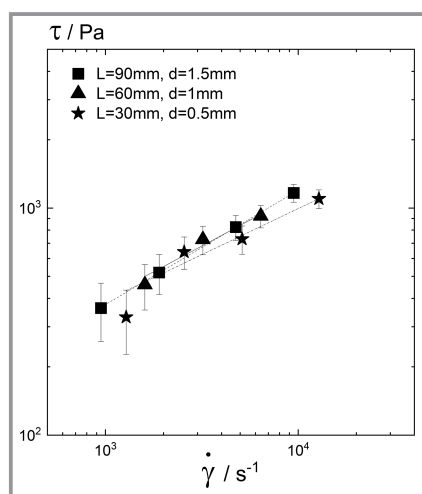


Figure 5. Flow behavior of alginate-based sample B measured with a capillary rheometer. Shear stress as a function of shear rate for different stainless steel nozzle sizes.

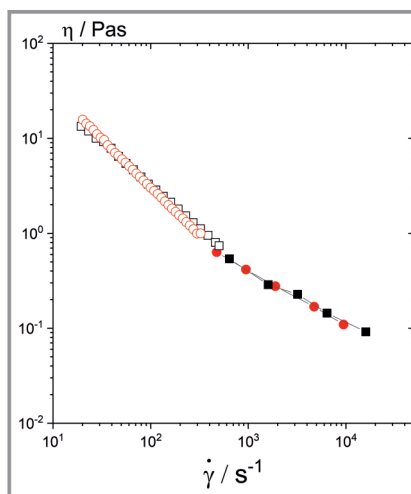


Figure 6. Viscosity η as a function of shear rate for alginate-based sample B (squares) and gelatin-based sample C (circles) as obtained from rotational rheometry with rough plates (open symbols) and capillary rheometry (closed symbols).

τ_y/τ_s in comparison to gelatin gels, emphasizing the strong slip of polysaccharide gels.

Samples B and C show similar yield stress (Fig. 7) and identical flow behavior (Fig. 6). However, they present contrasting slip performance at low stresses, as previously discussed. In addition, slip is not significant for both gel types at high shear stress or high shear rate.

3.4 3D Printing Experiments

Next the printing quality accessible with alginate and gelatin samples B and C, respectively, was compared, both exhibiting similar rheological properties and no slip at high stress relevant for printing. These two samples were 3D printed using needles of different materials. The lowest pressure necessary for printing continuous lines without interruptions or defects was found to be 0.17 MPa

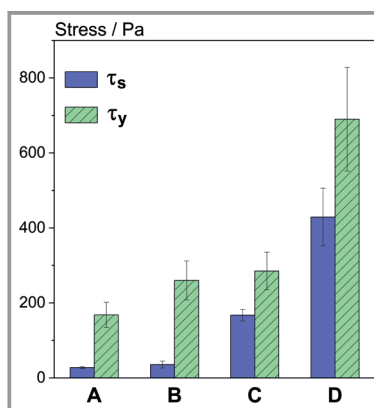


Figure 7. Slip stress τ_s (blank columns) with steel plate and yield stress τ_y (patterned columns) for samples A–D.

for alginate-based sample B and, surprisingly, only 0.1 MPa for gelatin-based sample C. These pressure values correspond to wall shear stress values of 598 and 359 Pa, respectively. The wall shear stress τ_w is given by Eq. (3):

$$\tau_w = \frac{\Delta P r}{2L} \quad (3)$$

Where ΔP corresponds to the pressure difference and r and L are the needle radius and length, respectively.

Overall, the use of different needle materials does not affect the printing quality of the constructs substantially (Fig. 8). This indicates that the no-slip boundary condition is valid not only for the stainless-steel nozzle as already confirmed by capillary rheometry (Fig. 5), but also for the nozzles made from lower surface energy polymer materials. This is further confirmed by the analysis of the printed lines. In order to evaluate filament formation, the spreading ratio of the lines was calculated as the line width divided by the nozzle outlet diameter. The spreading ratio values for alginate-based sample B lines printed with steel, PP and PTFE needles are 5.1 ± 1.2 , 5 ± 1 , and 4.6 ± 1.2 , respectively, whereas gelatin-based sample C shows spreading ratio values of 3.9 ± 0.5 for steel needles and 4.3 ± 0.5 for both PP and PTFE needles.

The pronounced slip effect observed at low shear stresses ($\tau < \tau_y$) is attributed to the different wetting behavior of the gels on different materials and thus may have an effect on the spreading of the first printed layer using different substrates. Lee et al. investigated the effect of printing platforms with varying surface energy on the line width of the printed constructs [31]. They found that hydrophobic substrates yielded thinner printed lines in comparison to hydrophilic printing platforms. This aspect was not followed up here.

The pronounced slip behavior of the alginate-based samples for $\tau < \tau_y$ is unexpected considering that these samples contain essentially just a trace amount of polymer. Wall slip

typically occurs in highly filled, dense suspensions [25]. Slip here may be interpreted as an indication of hydrogel phase separation and/or formation of structural micro-heterogeneities. The alginate gels may be treated as suspensions of micro-gel particles in a low viscosity aqueous polymer solution. The printed lines of the alginate sample B are irregular and non-uniform in comparison to the ones printed from gelatin sample C, as shown in Fig. 8. This effect is more evident in Fig. 9, where the variation of line width is plotted as a function of the position x along a printed strut.

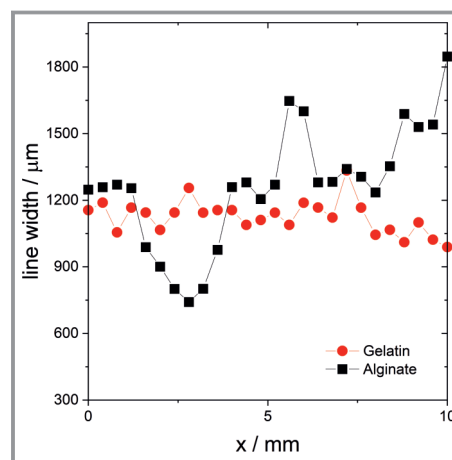


Figure 9. Filament width as a function of the position along a printed filament for alginate-based sample B (squares) and gelatin-based sample C (circles).

The pronounced fluctuations in printed filament width observed for sample B as well as the need of a higher pressure to print continuous lines in comparison to sample C could be interpreted as a consequence of the hydrogel micro-heterogeneity suggested by the pronounced low-stress slip behavior found for the alginate gels. The characterization of such micro-heterogeneities in cell carrier hydrogels will be addressed in detail in a subsequent study.

In several previous studies the yield stress of bioinks is correlated to printing quality [32–34]. In order to investigate the effect of yield stress on printing quality for the hydrogels investigated here, 20-layer objects were printed using a stainless-steel nozzle (Fig. 10). Printing of multi-layered constructs from sample A was not possible due to its lack of elasticity and low yield stress. Tab. 2 summarizes slip stress, rheological parameters as well as printing pressure of hydrogels B–D.

Samples B and C exhibit similar yield stress, while that of sample D is almost three times higher. This seems to have an effect on the top surface geometrical accuracy of the printed constructs (Figs. 10a–c). Sample D shows lower line spread ratio (Tab. 3), i.e., superior shape fidelity in comparison to samples B and C, presumably

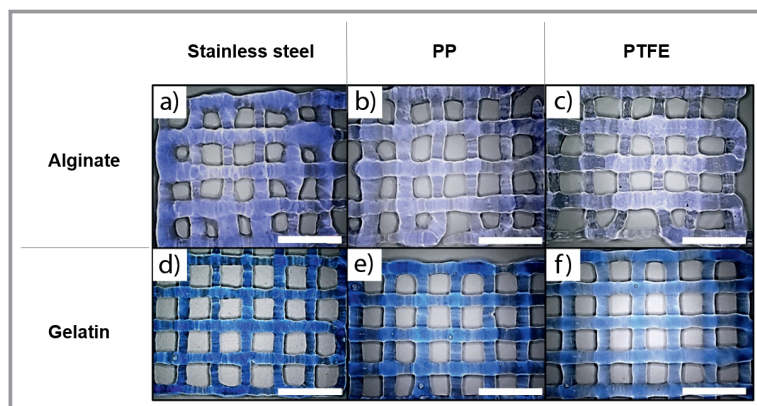


Figure 8. 3D printed constructs. Upper row represents alginate-based sample B printed at 0.17 MPa and bottom row gelatin-based sample C printed at 0.1 MPa. Hydrogels were printed with stainless steel nozzle (a) and (d), PP nozzle (b) and (e), as well as PTFE nozzle (c) and (f). Outlet diameter of all nozzles is $250 \mu\text{m}$. Scale bar: 5 mm.

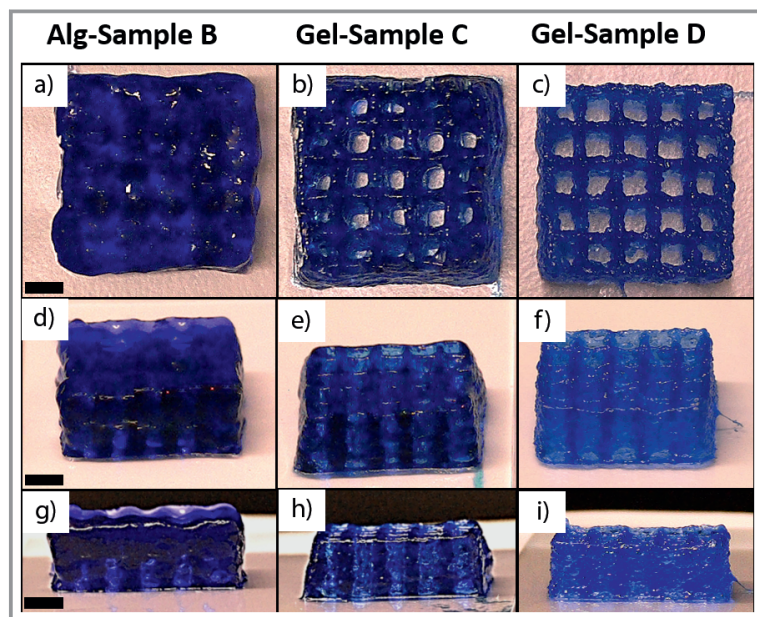


Figure 10. 3D printed 20-layer log-pile constructs, total area $\sim 15 \times 15 \text{ mm}^2$, height $\sim 5 \text{ mm}$. a), d), and g) refer to alginate-based sample B; b), e), and h) represent gelatin-based sample C; c), f), and i) gelatin-based sample D. Scale bar: 3 mm.

Table 2. Slip stress, yield stress, elastic modulus G_0 , minimum printing pressure and corresponding wall shear stress for samples B-D.

| | Slip stress [Pa] | Yield stress [Pa] | G_0 [Pa] | Pressure [MPa] | Wall shear stress [Pa] |
|----------|------------------|-------------------|----------------|----------------|------------------------|
| Sample B | 36 ± 9 | 260 ± 52 | 1900 ± 380 | 0.17 | 598 |
| Sample C | 167 ± 15 | 280 ± 50 | 285 ± 40 | 0.10 | 359 |
| Sample D | 429 ± 77 | 690 ± 138 | 1550 ± 310 | 0.24 | 837 |

due to the higher yield stress. The poor top surface fidelity of sample B can be attributed to the inhomogeneous filament formation and higher spread ratio.

Samples B and D show a better layer stacking quality in comparison to sample C (Figs. 10d–i). Possibly due to their higher elastic modulus values ($G_0 > 10^3 \text{ Pa}$) in comparison to gel C ($G_0 \sim 285 \text{ Pa}$), a more pronounced filament merging is observed for sample C, yielding a smaller top surface length in comparison to the bottom length of the 3D construct (Tab. 3). The low elasticity of this hydrogel and hence

Table 3. Printability parameters for samples B-D.

| | Line spread ratio | Top surface length [mm] | Log pile height [mm] | Layer height [μm] |
|----------|-------------------|-------------------------|----------------------|--------------------------------|
| Model | 1 | 15 | 5 | 250 |
| Sample B | 5.1 ± 1.2 | 15.6 ± 1.5 | 5.9 ± 0.2 | 295 ± 10 |
| Sample C | 3.9 ± 0.5 | 13.8 ± 0.6 | 5.2 ± 0.1 | 260 ± 4 |
| Sample D | 3.3 ± 0.6 | 15.3 ± 0.5 | 5.4 ± 0.1 | 270 ± 7 |

its poor resistance against gravitational sagging seems to cause layer collapse, resulting in multi-layered constructs with lower height.

In this study, a high elastic modulus G_0 yields a better layer stacking quality (samples B and D) while a higher yield stress is related to an improved filament formation and shape fidelity (sample D). This is in line with an earlier study using collagen hydrogels as printing ink reporting high printing quality for $G_0 > 1000 \text{ Pa}$ [35]. Besides, gel elasticity has to be adjusted to regulate matrix stiffness and cell proliferation [8]. Extremely high yield stresses, however, can lead to difficulties incorporating living cells or may cause nozzle clogging [34, 35]. Lee et al. suggested a maximum yield stress value of 1000 Pa for collagen-based hydrogels allowing for extrusion through a nozzle of 400 μm diameter [35]. It should be noted that sample D ($\tau_s \sim 690 \text{ Pa}$) needs a higher extrusion pressure for continuous filament printing in comparison to samples B and C ($\tau_s < 300 \text{ Pa}$, Tab. 2). A higher yield stress, and therefore higher printing pressure, results in a higher shear stress (Eq. (3)) experienced by the living cells while passing through the needle. This can lead to cell damage and low cell viability after printing [36, 37].

4 Conclusion

Herein wall slip, flow behavior, and elasticity of alginate as well as gelatin-based hydrogels with respect to the impact of these rheological and wetting properties on extrusion-based bioprinting (EBB) was investigated. At stresses below the yield stress τ_y , rotational rheometry revealed that alginate-based hydrogels presented stronger slip than gelatin samples, irrespective of crosslinker and polymer concentration. Slip at low stresses is more pronounced on PP and PTFE plates than on stainless steel plates for all samples. Capillary rheometry and printing tests using nozzles made from different materials (stainless steel, PP, and PTFE) confirm that slip is negligible at stresses $\tau > \tau_y$ relevant for EBB. The strong slip at low stresses observed for the alginate gels, however, is indicative of a heterogeneous microstructure, presumably comprising a dense suspension of microgel particles in a low viscosity polymer solution. This seems to show up in the printing results when comparing an alginate gel and a gelatin sample with similar yield stress and viscosity. The presumably heterogeneous alginate sample requires a higher extrusion pressure for printing uninterrupted lines and even more importantly exhibits strong fluctuations in line width and a higher line spread ratio. This striking observation demands further systematic investigations regarding the relevance of ink heterogeneity for printing quality

and also cell viability. Finally, the EBB experiments confirmed that a higher yield stress of the bioink requires a higher extrusion pressure but improves the shape fidelity of multilayered 3D constructs, while increasing gel elasticity enhanced layer stacking quality.

The authors would like to thank Dr. Bernhard Hochstein for the fruitful discussions on this research work. Open access funding enabled and organized by Projekt DEAL.

Symbols

| | | |
|------------|-----------------------|--------------------------------|
| t_c | [s] | characteristic time constant |
| d | [m] | diameter |
| h | [mm] | gap height |
| L | [m] | length |
| G_0 | [Pa] | plateau shear modulus |
| n | [s ⁻¹] | plate rotational velocity |
| x | [mm] | position along a printed strut |
| r | [mm] | radius |
| R_z | [μ m] | roughness |
| V_s | [mm s ⁻¹] | slip velocity |
| G' | [Pa] | storage modulus |
| ΔP | [Pa] | pressure difference |

Greek symbols

| | | |
|----------------|--------------------|------------------------------|
| γ | [-] | true elastic deformation |
| $\dot{\gamma}$ | [s ⁻¹] | shear rate |
| γ_{app} | [-] | apparent elastic deformation |
| η | [Pa s] | shear viscosity |
| τ | [Pa] | shear stress |
| τ_s | [Pa] | slip stress |
| τ_w | [Pa] | wall shear stress |
| τ_y | [Pa] | yield stress |

Abbreviations

| | |
|------|-----------------------------|
| GDL | D-Glucono-1,5-lacton |
| EBB | extrusion-based bioprinting |
| PP | polypropylene |
| PTFE | polytetrafluoroethylene |
| PVA | poly(vinyl alcohol) |

References

- [1] W. L. Ng, C. K. Chua, Y. Chen, *Prog. Polym. Sci.* **2019**, *97*, 101145. DOI: <https://doi.org/10.1016/j.progpolymsci.2019.101145>
- [2] N. Ashammakhi, S. Ahadian, C. Xu, H. Montazerian, H. Ko, R. Nasiri, N. Barros, A. Khademhosseini, *Mater. Today Bio* **2019**, *1*, 100008. DOI: <https://doi.org/10.1016/j.mtbio.2019.100008>
- [3] G. Cidonio, M. Glinka, J. I. Dawson, R. O. C. Oreffo, *Biomaterials* **2019**, *209*, 10–24. DOI: <https://doi.org/10.1016/j.biomaterials.2019.04.009>
- [4] K. Duval, H. Grover, L. Han, Y. Mou, A. Pegoraro, J. Fredberg, Z. Chen, *Physiology* **2017**, *32* (4), 266–277. DOI: <https://doi.org/10.1152/physiol.00036.2016>
- [5] W. L. Ng, J. M. Lee, M. Zhou, Y. Chen, K. A. Lee, W. Y. Yeong, Y. Shen, *Biofabrication* **2020**, *12*, 022001. DOI: <https://doi.org/10.1088/1758-5090/ab6034>
- [6] X. Li, B. Liu, B. Pei, J. Chen, D. Zhou, J. Peng, X. Zhang, W. Jia, T. Xu, *Chem. Rev.* **2020**, *120* (19), 10793–10833. DOI: <https://doi.org/10.1021/acs.chemrev.0c00008>
- [7] I. T. Ozbolat, M. Hospodiuk, *Biomaterials* **2016**, *76*, 321–343. DOI: <https://doi.org/10.1016/j.biomaterials.2015.10.076>
- [8] D. Chimene, R. Kaunas, A. K. Gaharwar, *Adv. Mater.* **2020**, *32*, 1902026. DOI: <https://doi.org/10.1002/adma.201902026>
- [9] J. Li, C. Wu, P. K. Chu, M. Gelinski, *Mater. Sci. Eng. R* **2020**, *140*, 100543. DOI: <https://doi.org/10.1016/j.mser.2020.100543>
- [10] G. Poologasundarampillai, A. Haweet, S. N. Jayash, G. Morgan, J. E. Moore Jr, A. Candeo, *Bioprinting* **2021**, *23*, 00144. DOI: <https://doi.org/10.1016/j.bprint.2021.e00144>
- [11] S. Wang, S. Ravindranath, P. E. Boukany, *Macromolecules* **2011**, *44* (2), 183–190. DOI: <https://doi.org/10.1021/ma101223q>
- [12] a) C. Xu, M. Fiess, N. Willenbacher, *IEEE J. Photovoltaics* **2017**, *7* (1), 129–135. DOI: <https://doi.org/10.1109/JPHOTOV.2016.2626147>; b) M. Sarker, X. B. Chen, *J. Manuf. Sci. Eng.* **2017**, *139* (8), 081002. DOI: <https://doi.org/10.1115/1.4036226>
- [13] B. Stoimenov, V. Fridrici, P. Kapsa, H. Kosukegawa, M. Ohta, *Tribology Online* **2013**, *8* (1), 140–52. DOI: <https://doi.org/10.2474/troll.8.140>
- [14] S. Aktas, D. M. Kalyon, B. M. Marín-Santibáñez, J. Pérez-González, *J. Rheol.* **2014**, *58* (2), 513–535. DOI: <https://doi.org/10.1122/1.4866295>
- [15] J. Leppiniemi et al., *ACS Appl. Mater. Interfaces* **2017**, *9* (26), 21959–21970. DOI: <https://doi.org/10.1021/acsami.7b02756>
- [16] S. Sakai, A. Yoshii, S. Sakurai, K. Horii, O. Nagasuna, *Mater. Today Bio* **2020**, *8*, 100078. DOI: <https://doi.org/10.1016/j.mtbio.2020.100078>
- [17] J. Emmermacher et al., *Biofabrication* **2020**, *12*, 025022. DOI: <https://doi.org/10.1088/1758-5090/ab7553>
- [18] J. Göhl, K. Markstedt, A. Mark, K. Hakansson, P. Gatenholm, F. Edelvik, *Biofabrication* **2018**, *10*, 034105. DOI: <https://doi.org/10.1088/1758-5090/aac872>
- [19] S. J. Müller et al., *PLOS ONE* **2020**, *15* (7), 0236371. DOI: <https://doi.org/10.1371/journal.pone.0236371>
- [20] M. G. Li, X. Y. Tian, X. B. Chen, *J. Manuf. Sci. Eng.* **2009**, *131* (3), 034501. DOI: <https://doi.org/10.1115/1.3123331>
- [21] M. Sarker, X. B. Chen, *J. Manuf. Sci. Eng.* **2017**, *139* (8), 081002. DOI: <https://doi.org/10.1115/1.4036226>
- [22] A. Yoshimura, R. K. Prud'homme, *J. Rheol.* **1988**, *32*, 53–67. DOI: <https://doi.org/10.1122/1.549963>
- [23] P. Coussot, *Rheophysics: Matter in All its States*, 1st ed., Springer, Berlin **2014**.
- [24] H. M. Shewan, J. R. Stokes, M. Cloitre, *Soft Matter* **2017**, *13*, 2099–2106. DOI: <https://doi.org/10.1039/C6SM01775D>
- [25] P. Coussot, *Rheometry of pastes, suspensions, and granular materials: applications in industry and environment*, 1st ed., Wiley, Hoboken, NJ **2005**.
- [26] T. G. Mezger, *The rheology handbook: for users of rotational and oscillatory rheometers*, 2nd ed., Vincentz Network, Hannover **2006**.
- [27] M. Mooney, *J. Rheol.* **1931**, *2*, 210–222. DOI: <https://doi.org/10.1122/1.2116364>

- [28] R. Matjie, S. Zhang, Q. Zhao, N. Mabuza, J. R. Bunt, *Fuel* **2016**, *181*, 573–578. DOI: <https://doi.org/10.1016/j.fuel.2016.04.105>
- [29] P. F. Rios, H. Dodiuk, S. Kenig, S. McCarthy, A. Dotan, *J. Adhes. Sci. Technol.* **2007**, *21* (3–4), 227–241. DOI: <https://doi.org/10.1163/156856107780684567>
- [30] K. Nayebzadeh, J. Chen, E. Dickinson, T. Moschakis, *Langmuir* **2006**, *22* (21), 8873–8880. DOI: <https://doi.org/10.1021/la060419o>
- [31] J. Lee, W. Y. Yeong, *Virtual and Physical Prototyping* **2015** *10* (1), 3–8. DOI: <https://doi.org/10.1080/17452759.2014.979557>
- [32] N. Paxton, W. Smolan, T. Böck, F. Melchels, J. Groll, T. Jungst, *Biofabrication* **2017**, *9*, 044107. DOI: <https://doi.org/10.1088/1758-5090/aa8dd8>
- [33] A. Schwab, R. Levato, M. D'Este, S. Piluso, D. Eglin, J. Malda, *Chem. Rev.* **2020** *120* (19), 11028–11055. DOI: <https://doi.org/10.1021/acs.chemrev.0c00084>
- [34] V. H. M. Mouser, F. P. W. Melchels, J. Visser, W. J. A. Dhert, D. Gawlitta, J. Malda, *Biofabrication* **2016**, *8*, 035003. DOI: <https://doi.org/10.1088/1758-5090/8/3/035003>
- [35] J. Lee, S. J. Oh, S. H. An, W. Kim, S. Kim, *Biofabrication* **2020**, *12*, 035018. DOI: <https://doi.org/10.1088/1758-5090/ab8707>
- [36] A. Blaeser, D. F. D. Campos, U. Puster, W. Richtering, M. M. Stevens, H. Fischer, *Adv. Healthcare Mater.* **2016**, *5*, 326–333. DOI: <https://doi.org/10.1002/adhm.201500677>
- [37] T. Billiet, E. Gevaert, T. De Schryver, M. Cornelissen, P. Dubruel, *Biomaterials* **2014**, *35* (1), 49–32. DOI: <https://doi.org/10.1016/j.biomaterials.2013.09.078>